Influence of crystallization parameters on guest selectivity and structures in a CO2-based separation process using TBAB semi-clathrate hydrates

Carla Rodriguez, Quang Du Le, Cristian Focsa, Claire Pirim, Bertrand Chazallon

Influence of Crystallization Parameters on Guest Selectivity and Structures in a CO_2-based Separation Process Using TBAB Semi-Clathrate Hydrates

Carla T. Rodriguez, Quang Du Le, Cristian Focsa, Claire Pirim and Bertrand Chazallon *

Université de Lille, CNRS, UMR 8523 – PhLAM – Physique des Lasers, Atomes et Molécules, CERLA – Centre d'Etudes et de Recherche Lasers et Applications, F-59000, Lille, France.

*Corresponding author. E-mail: bertrand.chazallon@univ-lille.fr
Tel: +33 (0)320636468

Abstract

Carbon dioxide (CO_2) capture from flue gas mixture analogs based on ionic clathrate hydrates crystallization (using tetra-n-butyl ammonium bromide, TBAB) is investigated by optical microscopy and Raman spectroscopy. The purpose of this research is to investigate the influence of the crystallization protocol (slow versus fast cooling/heating) on the subsequent semi-clathrate structures formed from a 35wt% TBAB-H_2O solution and CO_2 separation efficiency from an initial gas mixture of 10%CO_2+90%N_2. *In-situ* Raman analyses reveal that structure type B (sometimes associated with several polymorph phases) is readily observed at the onset of the formation process regardless of the crystallization protocol. Structure type B remains stable up to a temperature close to that of dissociation, whereas polymorphs form and evolve continuously until then. Just before dissociation, structure type A is additionally observed. The protocol involving slow cooling and heating steps (similar to the isochoric pressure search method) performs slightly better in terms of selectivity than the one using the multi-cycling temperature approach (fast cooling and heating). However, within the same protocol, the selectivity greatly depends on the specific semi-clathrate structures formed. We find that the best CO_2 selectivity is achieved when structure A is formed compared to all other semi-clathrate phases.

Keywords: Semi-clathrate hydrates; Raman spectroscopy; CO_2 capture; Tetra-n-butyl ammonium bromide.

1. INTRODUCTION

Significant efforts have been made to mitigate greenhouse gases emissions, in particular for carbon dioxide (CO_2) emitted from human activities. These emissions represent an imminent threat for the atmosphere, causing diverse environmental damages [1]. Even though the development of renewable sources for energy production is now of international concern, global anthropogenic CO_2 emissions are still dominated by the burning of fossils fuels [2].

Over the last two decades, new global warming and climate change mitigation strategies provided the incentive for the development of Carbon Capture and Storage (CCS) technologies. Their main goal is to trap the large amounts of CO_2 released into the atmosphere by industrial combustion processes. In such processes, CO_2 gas is emitted in either one of these three stages: pre-combustion, oxy-combustion, or post-combustion [1]. This paper focuses on post-combustion sequestration, i.e., on CO_2 capture once the burning process of fossil fuels is completed [3,4]. Gas sequestration can be achieved through many different separation approaches, such as: chemical absorption (e.g. Monoethylamine (MEA)-based absorption process) and its optimization [5–10], physical and chemical adsorption [11], membrane-based separation processes [4,9,10,12], and cryogenic processes [1,13]. However, previous research works have shown several drawbacks for these methods. For instance, they require a massive amount of energy, involve high operating and capture costs, and present risks of degradation, corrosion, oxidation, and environmental pollution [4,14]. Questions have been raised about their efficiency and consequently, investigations with objectives to find greener CCS solutions have become essential.

As an alternative solution, the CCS technology involving Hydrate-Based Separation Processes (HBSP) is of current interest [3]. The principal elements of HBSP are clathrate hydrates. They consist of hydrogen-bonded water molecules that form solid (crystalline) enclosures able to "host" small gas molecules such as methane (CH_4), carbon dioxide (CO_2), nitrogen (N_2), hydrogen (H_2), etc., as "guests", under certain pressure and temperature conditions [15]. Therefore, clathrate hydrates crystallize in different structures and under different thermodynamic conditions depending on the molecular size of the guest hosted inside the water cages [16]. The thermodynamic conditions can be improved (i.e., softened to minimize energy costs) by adding other compounds to the network of water molecules. Such so–called additives become either guest molecules in water enclosures, or (sometimes and) participate in the water structure itself, forming semi-clathrate (*sc*) hydrates in this latter case [17].

The first discussions and analyses of *sc* hydrates began in 1940 with Fowler et al. [18]. The authors focused on quaternary ammonium salts as foreign molecules participating in *sc* hydrates. Subsequent researches by e.g., Shimada et al., 2003, [19], have found that these salts can work as promoters, i.e., induce an important pressure reduction in the equilibrium hydrate formation pressure applied for CO_2 capture [20–22]. Among all additive compounds studied by the authors, tetra-n-butyl ammonium salts not only presented a high solubility, but also allowed hydrates to dissociate at higher temperatures [23]. Furthermore, utilizing tetra-n-butyl ammonium bromide (TBAB) as an additive for hydrate formation enabled the system to be highly selective toward CO_2 [24], provided better efficiency and stability for CO_2 separation compared to clathrate hydrates formed with no additives [21,25], and finally generated a TBAB-H_2O mixture more

compatible with the environment (when recovered [26,27]) compared to other commonly used chemical absorbents [14].

It should be noted that the structures of TBAB-H_2O differ from the well-known structures I, II, and H of gas hydrates [17]. A considerable amount of discussions about the structure and composition of TBAB-*sc* without guest gases and under atmospheric pressure have been reported in the literature [17,20,28–33]. The TBAB-*sc* consists of a hydrophilic bromide anion (Br^-) located at the vertices of the water host lattice, whereas the hydrophobic TBA^+ cation is centered in two fourteen-faced ($5^{12}6^2$) and two fifteen-faced ($5^{12}6^3$) polyhedra [17]. This means that only the small cages (twelve-faced polyhedra (5^{12})) are empty and available to store guest-gas molecules. Two main structures have been reported for TBAB-*sc*: a type A, showing a tetragonal crystal structure, and a type B, exhibiting an orthorhombic crystal structure [17,20,28–30,32,33]. Their hydration numbers ($(C_4H_9)_4N^+Br^-\bullet nH_2O$) have been extensively discussed in the literature. While a good agreement across the scientific literature exists for n=38 as the hydration number of structure type B (orthorhombic structure) at a stoichiometric concentration of about 32 wt.% [17], uncertainties regarding the hydration number associated to type A still remain. The works of Shimada et al. (2003) [19], Oyama et al. (2005) [30], and Shimada et al. (2005) [34] found a hydration number of n=26 at a stoichiometric concentration of 40 wt.% for type A, whereas Sato et al. (2013) rather estimated the hydration number to lie between n=30 and n=33 for a stoichiometric composition ranging from 35 wt.% to 37 wt.% (considering a congruent melting point at 286 K) [32]. Hydration numbers ranging between n=24 and n=32 have also been found in diffraction works from Rodionova et al. (2013) [31] and Jeffrey & Mc Mullan (1959) [28]. Recently, Oshima et al., 2018, [33] re-investigated the structure-composition relationship and concluded that

type A is tetragonal with hydration numbers linearly increasing from *n*=26 to *n*=28 as the TBAB initial content decreases from 40 wt.% to 20 wt.%.

Raman spectroscopy has been successfully applied to identify and discriminate structure types in TBAB-*sc*. Chazallon and coworkers showed in a previous work [20] that type A exhibited less peaks (8 peaks) in the C-H stretching mode region (~2600-3050 cm^{-1}) than type B (10 peaks). Other differences emerged in the authors' Raman spectra when comparing the two structures. While they observed a wide band centered at ~1323 cm^{-1} in type A TBAB-*sc*, two distinct bands (~1309 and ~1327 cm^{-1}) were rather observed in type B TBAB-*sc*. In addition, several shifts in band positions in the 90-600 cm^{-1} spectral region [20] have been identified. Once structure types A and B were unambiguously identified for TBAB-*sc*, several works further showed that the encapsulation of guests could modify the initial structure type and result in the coexistence of (new) mixed structures (polymorphism) featuring a combination of orthorhombic and tetragonal phases [20,35,36]. Specifically, Chazallon and coworkers [20] reported that the encapsulation of CO_2 or N_2 could induce unexpected structural changes of the initial structure, leading to the formation of type A, B, or new phases (polymorphs), all depending on the initial pressure (p), temperature (T), and TBAB concentration conditions. The authors observed structural changes from tetragonal to orthorhombic upon CO_2 enclathration under conditions of $p > 2$ MPa, whereas both structures were identified below $p < 2$ MPa [20]. In fact, the co-existence of a new polymorph phase was obtained under conditions of $p = 1.6$ MPa and $T = 283.4$ K, respectively. The new phase was characterized by two new bands emerging at 2959 cm^{-1} and 2979 cm^{-1}, respectively, and a band slightly shifted to 3020 cm^{-1} compared to a pure type B formed in CO_2-5wt.%TBAB-H_2O. Muromachi et al., 2014 [35] and Zhou et al., 2018 [37] identified via single crystal X-

rays and powder X-ray diffraction measurements the existence of a modified type B (with space group *Imma*, i.e. the same point group as the one of TBAB:38H_2O (*Pmma*) but a different lattice) when CO_2 is encapsulated in CO_2-TBAB-H_2O with TBAB concentrations ranging from 10 to 40 wt%. This confirmed the *sc*-structure modification induced by guest-encapsulation and observed by Raman spectroscopy [20].

CO_2-based gas mixtures trapped in TBAB hydrates show potential applications for CO_2 selectivity and capture processes in industry. Large-scale flue gas emissions released by thermal power plants are generally constituted of a mixture of carbon dioxide (CO_2) and nitrogen (N_2), with a concentration of CO_2 ranging between 3-15% [3,14,38,39]. While several communications have reported the structure and equilibrium properties of either pure CO_2 or N_2 TBAB-*sc* using different experimental techniques [20,22,40], the equilibrium properties of mixed CO_2 + N_2 TBAB-*sc* [41–43] have mainly been investigated using low concentrations of TBAB, i.e., ≤ 32 wt.%, the stoichiometric concentration corresponding to the stability domain of the orthorhombic phase. Evidences of the coexistence of structure A and B have been reported for mixed CO_2+N_2-TBAB-*sc* [44], whereas the structures of several quaternary salts used for the separation of CO_2+N_2 gas mixtures have been shown to crystallize in one of either of the orthorhombic or the tetragonal system. Moreover, Raman spectra of CO_2+N_2-32wt.%TBAB-H_2O and CO_2+N_2-20wt%TBAB-H_2O formed at T= 211 K and T= 200 K, respectively, were compared by Hashimoto et al., 2017 [44]. The authors observed the emergence of a modified phase with partial resemblance to both the orthorhombic and tetragonal structures and suggested the existence of a biphasic phase. As different structure types can feature distinct selectivity properties, the formation of such polymorphism may impact the resulting selectivity of the system. Accordingly, several studies addressed this matter and derived the Separation Factor (S.F.) of this

complex system, which reflects how selective the system is toward CO_2 enclathration from an initial binary CO_2/N_2 gas mixture [24,40]. However, S.F. of 21.4 [24] and 5.7 [44] have been obtained under the same p, T, and TBAB concentration conditions (32 wt.% TBAB, p = 1 MPa, T = 282.2 K), but for *sc* produced through different formation protocols. It yet remains unclear how TBAB-*sc* formation protocols can affect the resulting selectivity of the system. While it is clear that TBAB-*sc* are ideal candidates for CO_2 capture from binary CO_2+N_2 gas mixtures [24], a deeper understanding of how *sc* formation conditions can govern specific structure formations with distinct selectivity (and gas capacity) properties is required to fully apprehend their effectiveness in trapping CO_2 gas. To the best of our knowledge, to date only one study [45] has reported the equilibrium and compositional data for a binary CO_2+N_2-TBAB-*sc* in the high TBAB concentration range (≥ 35wt.%). Therefore, large unknowns still remain regarding the relationship between crystallization parameters, structure (hydration number), and CO_2 capture efficiency.

Our work focuses on flue gas analogs composed of a 10%CO_2 + 90%N_2 gas mixture enclathrated within a 35 wt.% TBAB-H_2O. We investigate and compare two CO_2+N_2-35wt%TBAB-H_2O formation protocols in terms of the resulting structure and selectivity, utilizing (1) the multi-cycling method [41], and (2) the isochoric pressure search method [21]. This approach will contribute to develop a better understanding of how structures generated with different formation protocols influence encapsulation mechanisms and selectivity.

2. MATERIALS AND METHODS

2.1. Sample preparation

The TBAB powder is provided by Sigma-Aldrich with a purity of ≥ 99.0% and is used without further purification treatment. A 35 wt.% TBAB aqueous solution is gravimetrically prepared utilizing an electronic balance (Sartorious basic BA 1100S, uncertainty of $\pm 10^{-5}$ mg) from a mixture of double distilled and de-ionized water (resistivity ~18 MΩ/cm^{-1}, Elgastat) in which TBAB powder is dissolved. The TBAB concentration is chosen based on the experiments conducted by Sato et al., 2013 [32], where the stoichiometric concentration was determined between 35wt% and 37wt% in TBAB-*sc*. Then, approximately 0.2 ml of TBAB + H_2O is deposited in the crucible of a high-pressure optical reactor. In a third step, the reactor is closed and the residual air is evacuated using a dry vacuum pump until primary vacuum is reached. Finally, the TBAB aqueous solution is exposed to a binary 10%CO_2 + 90%N_2 gas mixture (Praxair) at room temperature under a pressure of 3.7 MPa. Once the pressure in the reactor is stable at 3.7 MPa, the reactor is then isolated from the gas cylinder. Hydrates crystallization is triggered using two different temperature protocols which are further detailed below. Supplementary details about sample preparation can be found in previous publications [20,46,47].

2.2. Apparatus

A thermostated bath connected to the reactor and working with a circulating fluid (LAUDA (±0.1 °C) or HUBER Petite fleur (±0.1 °C)) controls the configuration of the temperature protocols. The temperature of the reactor is monitored via a K-type thermocouple (±0.3 °C) in direct contact with the reaction chamber. Variations of pressure are controlled with a high-pressure transducer (Keller, (0-200) ± 0.1 MPa)). Thermocouple and transducer data are continuously recorded on a data logger (Graphtec GL-200A).

Direct information on sample structure and composition is obtained by Raman analysis. The sample is irradiated using a DPSS Laser at 514.5 nm that is focused on the surface, through a x50 ULWD Olympus objective mounted on a BXFM microscope (Olympus). The scattered photons are collected using an Invia Reflex Raman spectrometer (Renishaw) coupled to the microscope. This allows non-destructive micro-probing of the three phases possibly constituting the samples (solid, liquid or gas) and optical monitoring of surface evolution during hydrates formation (i.e., the monitoring of superficial changes occurring with temperature variations). The spectral resolution is ~ 4 cm^{-1} using the 1800 grooves/mm diffraction grating. Gas phase spectra were recorded for 2 minutes, whereas solid phase spectra were recorded for 5 minutes each. Raman measurements of the gas phase are repeated two to three times to improve the statistics and Raman spectra of the *sc* are acquired at a maximum of 5 distinct positions on the hydrate's surface. Note that the positions from which Raman spectra are acquired are not indicated on the optical images shown in Figure 2, as distinct objectives are used for the collection of optical images and the acquisition of Raman spectra. The equipment is calibrated against the stable signature of a silicon standard at 520 ± 0.4 cm^{-1}. Raman bands are baseline-corrected and peak areas are integrated using Voigt profiles (or mixed Lorentzian-Gaussian profiles).

2.3. Temperature protocols

As mentioned before, the samples are exposed to two different temperature protocols that have been often utilized in hydrates formation processes. On the one hand, a fast cooling ramp (~5 K/min) is applied to induce rapid crystallization of the solution (protocol 1). On the other hand, a slow ramp is applied until

crystallization of the solution occurs (protocol 2). In both approaches (protocol 1 and protocol 2, see Figure S1 in the supplementary material), the temperature variations are always made within the *sc* stability domain, facilitating the production of hydrates from aqueous solution. Raman data and optical images are first collected at different sub-cooling, starting at $\Delta T_{sub} \sim 6.5$ K (where ΔT_{sub} is the difference between the measured temperature and the dissociation temperature) up to $\Delta T_{sub} \sim 0.5$ K, the latter being close to the hydrate's dissociation temperature.

Protocol 1 (fast cooling): 0.12 mL of the 35wt%TBAB-H_2O aqueous solution is subjected to a multi-cycling fast cooling protocol, where it is first quickly cooled down from 289 K to 258 K and then heated back up to 288.5 K, four times. This protocol is commonly utilized for hydrates formation [41]. These four cycles are then followed by eight heating-cooling cycles where the temperature is varied from 258 K to 281 K. Measurements start at 281 K up to the dissociation temperature, with steps of 0.5 K and a minimal equilibrium time of 14 hours between two temperature steps.

Protocol 2 (slow cooling): a new batch of 0.12 mL of the same mother solution is exposed to a step-by-step "slow" cooling protocol from ambient temperature to 266.5 K in steps of 1 K. The solution is allowed to equilibrate for 6 hours between each temperature. This protocol (see Figure S1) resembles that commonly used in blind reactors in isochoric-pressure search methods [48]. Then, the sample is heated up to 281.1 K by steps of 6 K (with still a minimal equilibrium time of 6 h) during which Raman measurements are performed. Once reached the temperature of 281.1 K, temperature steps are reduced and the dissociation temperature is approached by steps of 1.5 K (with a minimum standstill time of 6 h between steps) until complete dissociation is observed.

3. RESULTS AND DISCUSSION

The influence of formation protocols on the system structure and selectivity is presented below. Raman analyses are performed *in-situ* to characterize both the structure and selectivity (separation factor) of (10%CO_2 + 90%N_2)-35wt.%TBAB-H_2O for each temperature protocol.

3.1. Phase diagram at dissociation temperatures

Figure 1 shows a phase diagram of the CO_2+N_2-TBAB-H_2O system for which the starting TBAB concentration is 40 wt.%. Dissociation curves derived from literature data are plotted for pure gases (CO_2-TBAB-H_2O and N_2-TBAB-H_2O), as well as for different initial (CO_2 + N_2) gas mixture concentrations. Pure N_2–TBAB-*sc* are less stable than pure CO_2–TBAB-*sc* (i.e., the dissociation enthalpy of CO_2–TBAB-*sc* (ΔH_{dis} ~ 396 J/g_{hyd}) is higher than that of N_2–TBAB-*sc* (ΔH_{dis} ~ 367 J/g_{hyd})) [41]. The equilibrium lines of CO_2+N_2–TBAB-*sc* are found between those of the two pure gases in the p-T diagram. Note that high initial salt concentrations imply better stability and results in a shift of the stability curves toward higher temperatures [21]. Furthermore, in mixed gas systems, the initial CO_2 concentration apparently impacts the structural stability; it results in *sc* samples with low CO_2 contents being less stable than those containing more CO_2 (Figure 1). Nevertheless, the equilibrium line of 25%CO_2+N_2–TBAB-*sc* was found very close to that of pure CO_2–TBAB-*sc* [41]. This surprising result is not discussed in the literature, but may be related to the availability of empty cavities in the TBAB-*sc* structure or to the formation of unexpected polymorphs. In fact, the ratio of dodecahedral 5^{12} cavities to TBAB molecules per unit cell is not equivalent in type A, B or

polymorph *sc* structures, and the relative amount of TBAB *versus* guest gases will perform differently in stabilizing a given *sc* structure. Note that *sc* with structures corresponding to type A or exhibiting polymorphism have either not been unambiguously determined or not determined at all.

Previous work have shown that 35wt.%TBAB-H_2O *sc* have a congruent melting point of ~13°C (286 K) and exhibit a tetragonal structure [32]. To our knowledge, no dissociation data exits for semi-clathrates formed with (10%CO_2 +90%N_2 - 35wt.%TBAB). A new experimental dissociation point (see Figure 1) is found at T = 287.8 ± 0.3 K regardless of the formation protocol. This dissociation point lies between those found for pure N_2–TBAB-*sc* (at 40wt.% TBAB) and from the binary mixture 20%CO_2+80%N_2–40wt.%TBAB.

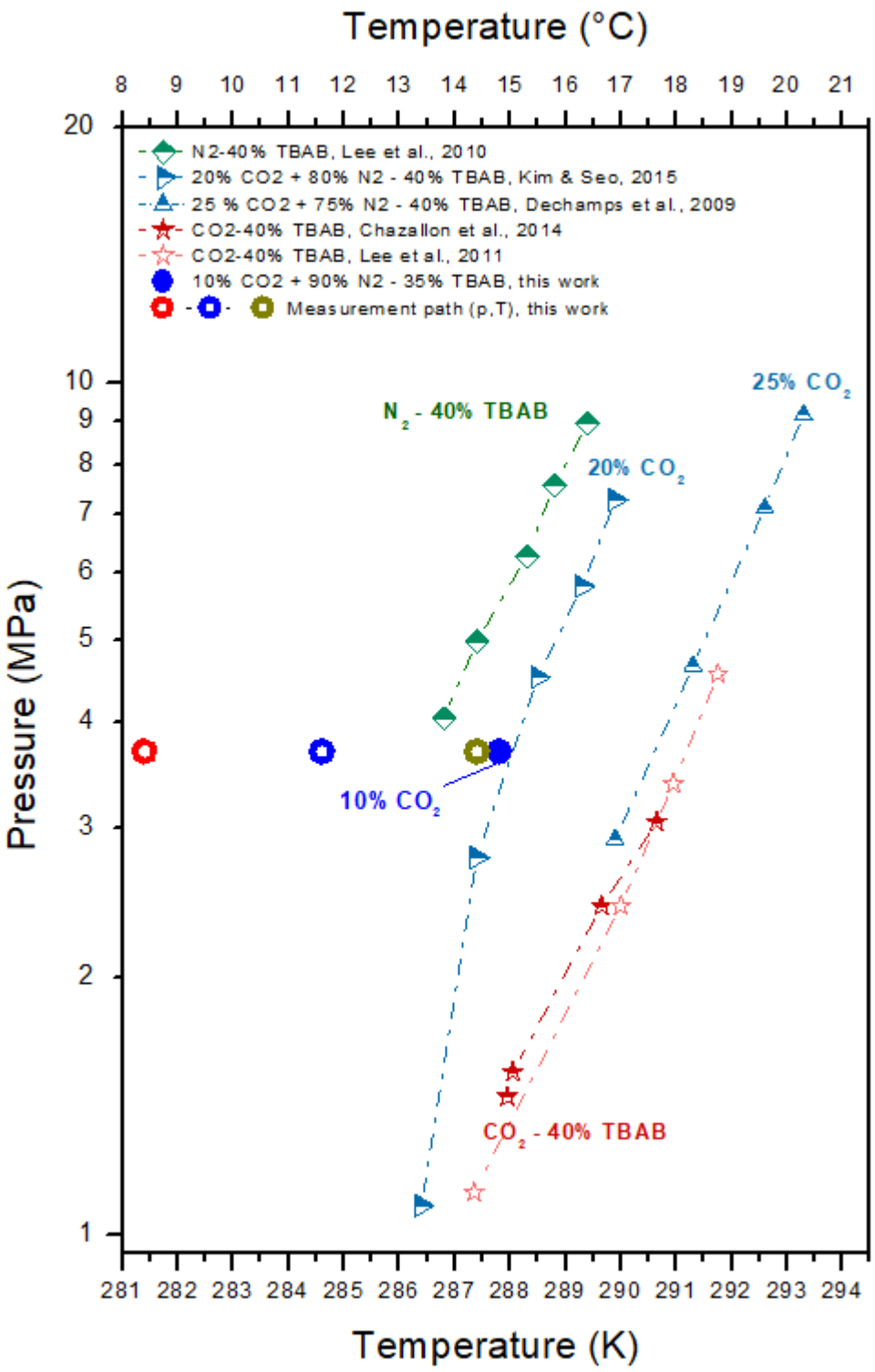

Figure 1: Phase diagram compiling literature data of the equilibrium dissociation lines compared to the dissociation temperature of the (10%CO_2 + 90%N_2) – 35wt.%TBAB + H_2O system (see legend and refer to references numbers

[20], [22], [41], [49], [45], for the works of Chazallon et al. (2014), Lee et al. (2011), Deschamps et al. (2009), Lee et al. (2010), Kim and Seo (2015), respectively). The path to dissociation is represented by open circles at T ~281 K, 284 K, and 287 K, at p=3.7 MPa.

3.2. Raman spectra for structure discrimination

Figure 2 compares *in-situ* Raman spectra that were collected in both protocols at different temperatures along the isobaric path leading to the TBAB-*sc* dissociation temperature (Figure 1). Three to five points are arbitrarily chosen in different areas of the sample surface for Raman analysis at each temperature step. Spectra covering the range of frequencies of TBAB C-H stretching modes (butyl groups, 2700 – 3050 cm^{-1}) are reported because they allow the discrimination of TBAB-*sc* structures [20,44]. Surface evolution with temperature is also monitored and the corresponding optical images are reported in Figure 2.

Between ~274 K and ~281.8 K, a rough surface with step-shaped crystals is observed in protocol 1, whereas polygonal-shaped crystals are obtained in protocol 2. On the basis of the TBAB-H_2O phase diagram alone, such morphology could correspond to the tetragonal phase [30]. However, it has been shown that the encapsulation of CO_2 in type A TBAB-*sc* can induce a phase transformation into a type B (orthorhombic structure) or a polymorph [20]. Therefore, the structure of TBAB-*sc* crystals cannot be unambiguously deduced from the optical image alone and necessitate the use of Raman spectroscopy, whereby unique signatures can be observed in the spectral region corresponding to the C-H stretching modes of TBAB-*sc*. As a result, the polygonal-shaped surface observed at 281.1 K in protocol 2 seems to reflect the sole presence of a type B, whereas the rough surface exhibiting step-shaped crystals observed at 281.8 K in protocol 1 bears

the signatures of both type B and polymorphic structures (referenced hereafter as Poly 1, Figure 2). The Raman signature of Poly 1 is close to that of type B observed in both protocols at T =281.1 K and 281.8 K, respectively, with however subtle changes in the relative intensity of the peaks located in the 2950-3025 cm^{-1} spectral region along with a weaker shoulder at 2866 cm^{-1}.

The surface morphology remains rough in both protocols when the temperature is increased from 281 K to 284.5 K. In protocol 1, Raman analysis reveals an evolution in surface structure: type B TBAB-*sc* is now observed to exist with a distinct polymorph (referenced as Poly 2 in Figure 2, protocol 1). The C-H signature of poly 2 is close to that of type B. Differences arise mainly in the emergence of weak bands at ~2961 cm^{-1} and ~2980 cm^{-1} and changes in the relative intensity of the peaks located in the 2950-3025 cm^{-1} spectral range for Poly 2 (see open diamonds, Figure 2 protocol 1). Poly 2 may correspond to the "new" phase reported previously [20]. In protocol 2, Poly 1 is the sole structure reported as no evidence of type B could be found.

After a standstill time of 6h at T =287.4 K, small crystals have nucleated (black dots, protocol 2 – reference time "t", Figure 2). This morphology is associated with the signature of a new polymorph (referenced Poly 3, protocol 2, T = 287.4 K) which is close to type A structure, with however small distinct features in the 2950-3025 cm^{-1} spectral range that are: i) a more prominent shoulder at ~2991 cm^{-1}, and ii) a small peak emerging at ~2969 cm^{-1}. In addition, a weak shoulder appears at ~2866 cm^{-1} (see open stars, Figure 2, protocol 2). Then, after an additional 72 h, the surface evolved into columnar crystals. Protocol 2 features then a mix of radially grown thin columns (possibly clustered) and columns with larger sections (Figure 2 at "t+72h"). Type B is known to grow with hexagonal plates evolving in an irregular columnar-

shaped morphology [50]. A needle-like morphology, evolving into columnar-shaped crystals, is also reported in type B formed from solutions at 19 wt.% TBAB. Moreover, high gas pressures (> 1MPa, such as in the present study (3.7 MPa)) increase the formation rate of TBAB-*sc* structures which results in polymorphisms with columnar-shaped crystals, varying distinctly in size and arrangement according to the nature of the ionic guests [44,50]. For instance, under conditions of p = 3.8 MPa and a sub-cooling of 5.7 K, CO_2–TBAB-*sc* form crystals with irregular shapes composed of thin columns assembled in clusters similar to those observed in type B TBAB-*sc* [50]. Similarly, under a sub-cooling of 2-4 K and high pressures (≥ 3 MPa) TBAB-*sc* exhibit smaller crystal sizes along with thin columns [44]. Therefore, we suggest that TBAB-*sc* crystals with clustered columns and polygonal shapes such as those reported in protocol 2 (T = 287.4 K, Figure 2) result from polymorphisms. This morphology continuously changes and TBAB-*sc* crystals are progressively replaced by a smooth (glancing) surface associated with the beginning of the dissociation when the temperature is slightly increased of 0.2-0.3 K (to T= 287.7 K) in an additional step (Figure 2, protocol 2). The corresponding Raman spectra show the concomitant emergence of structure types A and B. Of note, the two different structures A and B occurred for the same x-y position but at different z positions.

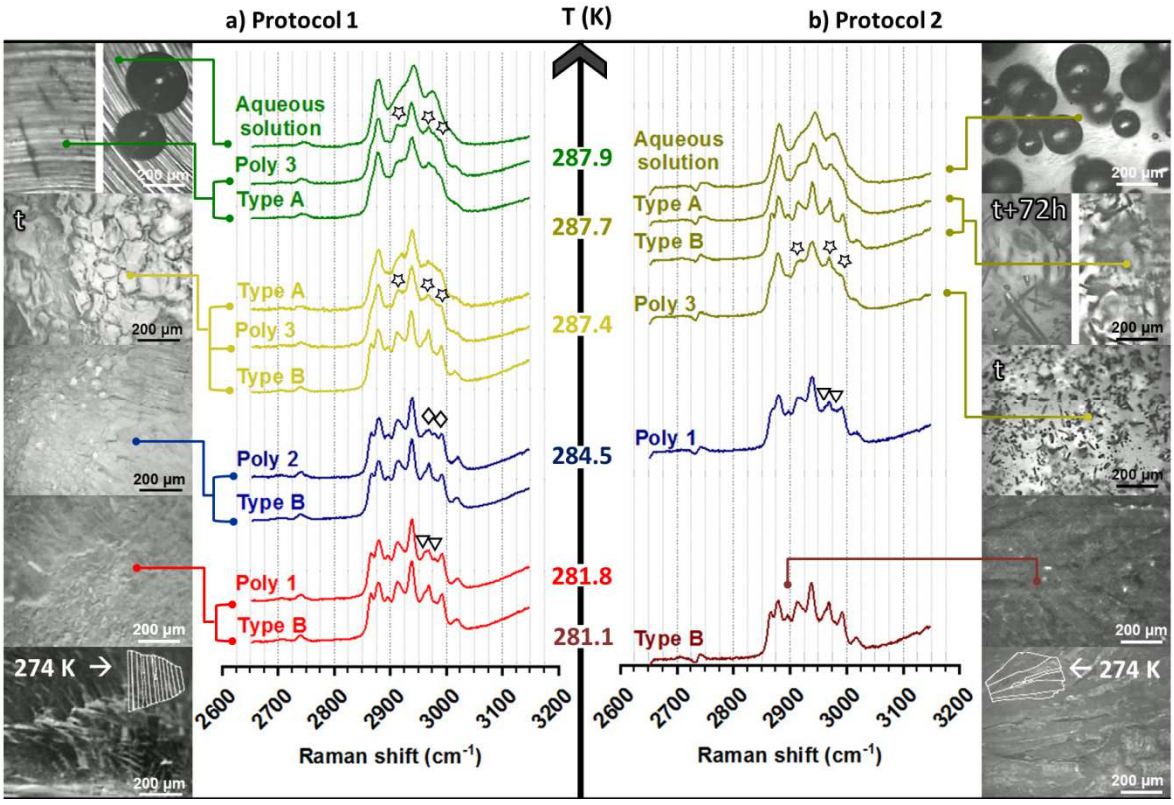

Figure 2: Comparison of the *in-situ* Raman analysis of TBAB C-H stretching modes for: a) Protocol 1 at T= 281.8 K, 284.5 K, 287.3 K and 287.9 K b) Protocol 2 at T= 281.1 K, 284.5 K and 287.5 K, both at p= 3.7 MPa. The letter "t" refers to the reference time (6h at 287.4 K in protocols 1 and 2) to which "t+72h" is compared. The latter indicates that the images and spectra were acquired after a standstill time of 3 days at the same temperature (287.4 K). Note that all other images and spectra are acquired after 6h of equilibrium time, but the letter "t" has been added only when comparison with a later time or comparison across protocols was needed. Symbols highlight spectral differences between Type B and Poly 1: ▽, Type B and Poly 2: ◇, Type A and Poly 3 : ☆.

In protocol 1, a temperature increase from 284.5 K to 287.4 K results in the formation of a patchy surface covered by large crystals (~ 100 µm) (Figure 2, protocol 1, 287.4 K). Raman measurements performed at T = 287.4 K show the occurrence of structure types A, B, and Poly 3, all three emerging concomitantly. The two different structures A and B are observed for the same x-y position but at different z

positions (as previously mentioned in protocol 2 for the same temperature range). Type B is reported close to the surface, whereas type A is generally observed below the surface. It has been observed earlier that CO_2-filled-TBAB-*sc* grew preferentially in solution rather than at the gas-liquid interface because of their higher density. It is thus conceivable that a TBAB concentration gradient exists during the growth, which promotes a guest-filled-type B (high hydration number of 38) at the surface and a guest-filled-type A below the surface (hydration number of ~26). It should be noted that each temperature protocol crosses the stability line of the canonical sI-CO_2+N_2 hydrate during its cooling cycles (down to 258 K or 265 K, depending upon the protocol) and furthermore involves temperatures low enough for simple guest-free TBAB-*sc* to form (empty–TBAB-*sc*). The latent heat of dissociation of empty–TBAB-*sc* -with structure type A is lower (ΔH_{dis} ~ 324 J/g_{hyd}) than that of CO_2-N_2–TBAB-*sc* (ΔH_{dis} ~ 390 J/g_{hyd}) [41], which confers greater stability to the latter. However, preferential growth for the empty–TBAB-*sc* below ~286 K is expected because TBAB performs better than either of its guest (CO_2 or N_2) in stabilizing crystal structures. All of this may well contribute to the micro-structural heterogeneity observed in the samples.

The signature of the liquid phase is observed in both protocols, after a few minutes at 287.7 K in protocol 2, and instantaneously at 287.9 K in protocol 1, the latter temperature being slightly above the dissociation temperature (287.8 ± 0.3 K, Figure 1). Upon dissociation of CO_2-N_2–TBAB-*sc*, gas bubbles containing CO_2 and N_2 are observed in the TBAB-*sc* aqueous solution.

In order to identify gas molecules trapped in TBAB-*sc*, we observed the characteristic Raman bands of CO_2 and N_2 in the spectral range covering the bending + C-C stretching modes of TBAB for CO_2 vibrational modes (1000 – 1600 cm^{-1}) (Figure 3), and for N_2 vibrational modes (2280 – 2370 cm^{-1}) (Figure

4). Specifically, at 3.7 MPa, the characteristic CO_2 free gas Raman bands are found at 1387.8 cm^{-1} and 1285.0 cm^{-1}, while that of N_2 is found at 2328.6 cm^{-1} (Table 1), in line with earlier measurements [20,47]. The gas trapped in the dodecahedral cages (5^{12}) of the hydrate can be identified because its Raman signatures are shifted toward lower frequencies (Table 1) with respect to the free-gas signature due to van der Waals interactions guests−TBAB-*sc* and guest−H_2O [20,44,51].

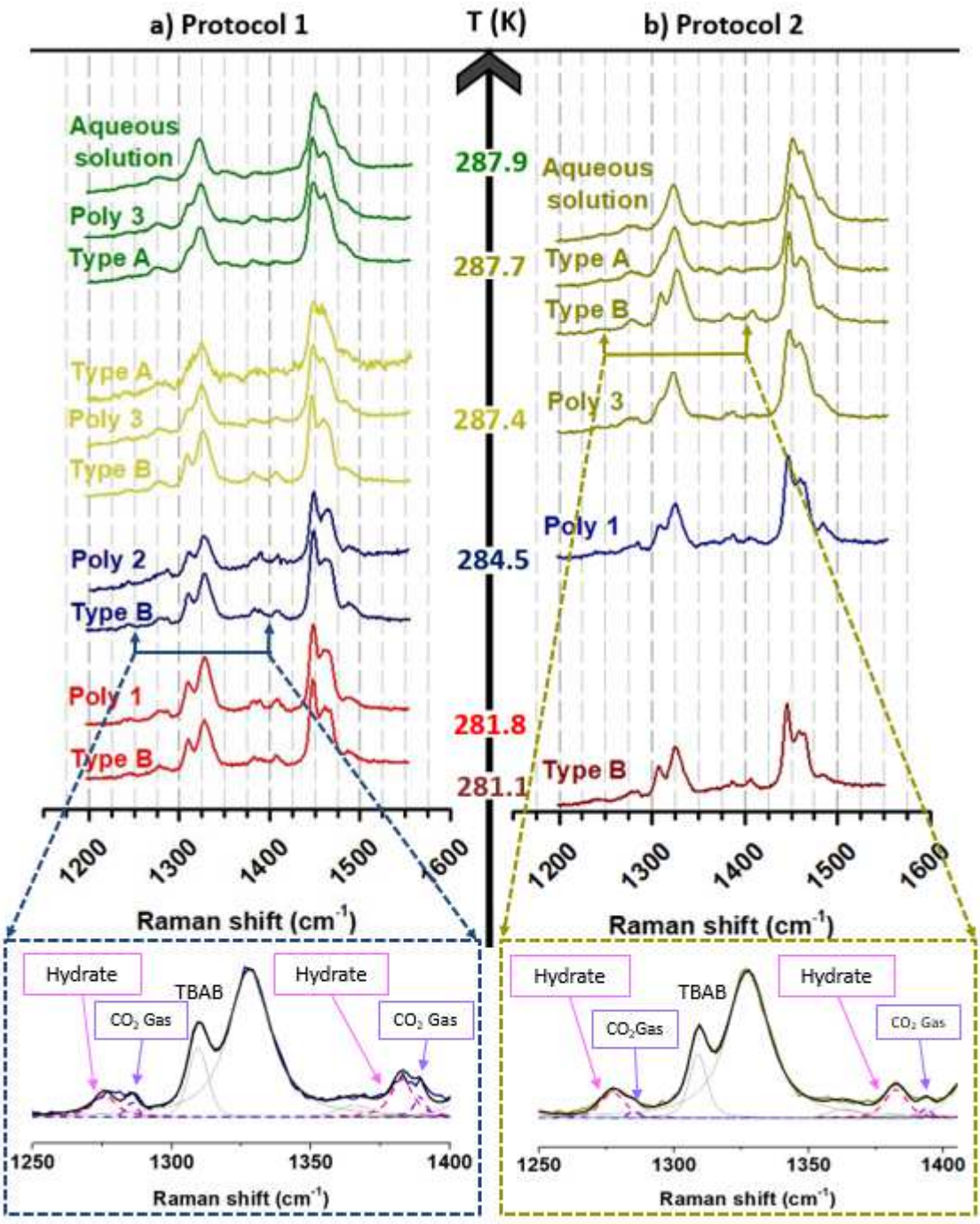

Figure 3: Comparison of the in-situ Raman analysis of TBAB bending modes + CO_2 vibrational modes for: a) Protocol 1 at T= 281.8 K, 284.5 K, 287.4 K and 287.9 K. b) Protocol 2 at T= 281.1 K, 284.5 K, 287.4 K and 287.7 K; both at p= 3.7 MPa.

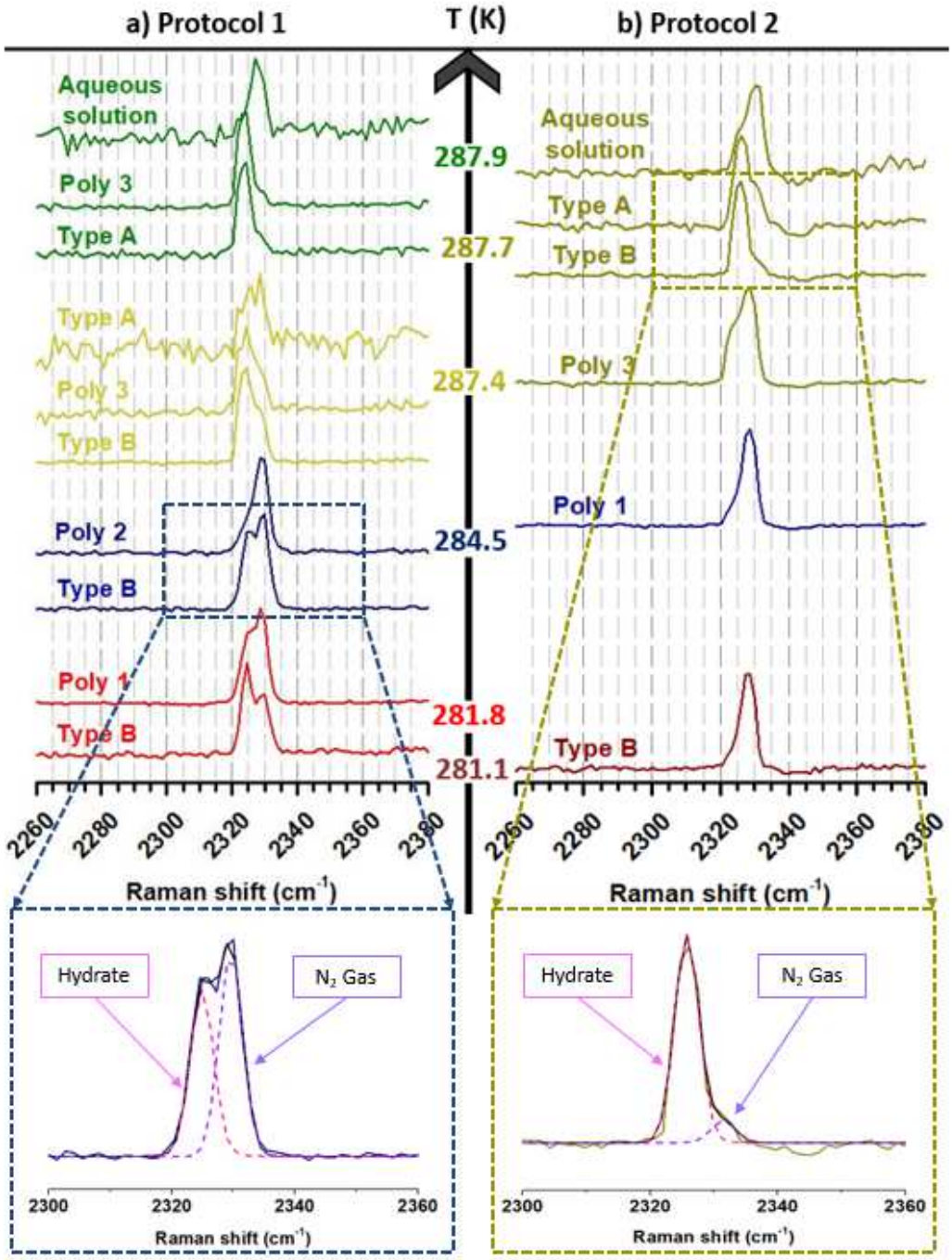

Figure 4: Comparison of the in-situ Raman analysis of N_2 stretching mode for both protocols at the same pressure (3.7 MPa) for: a) Protocol 1 at T= 281.8 K, 284.5 K, 287.4 K and 287.9 K. b) Protocol 2 at T= 281.1 K, 284.5 K, 287.4 K and 287.7 K.

A spectral deconvolution procedure is applied to the hydrates' Raman signatures to extract the contribution of guests (Figure 3 and 4). In the N_2 stretching region, the relative contribution of enclathrated N_2 to N_2 free gas (originating mainly from the solid-gas interface) can be derived from a simple 2-band fit (see inset in Figure 4). However, as the CO_2 Fermi resonance spectral region overlaps that of the TBAB C-C bending/stretching region, four bands are used to extract the enclathrated CO_2 and CO_2 gas (when present) contributions from that of TBAB, for which eight bands are identified (the inset presented in Figure 3 shows an enlarged portion of the spectral region between 1250-1400 cm^{-1}). These measurements are then used to derive the system's selectivity toward CO_2.

Table 1: Raman gas (N_2 and CO_2) and guest band frequencies (and associated full width at half maximum (FWHM)) in the main *sc*-phases (type A and type B). All spectra have been collected with a spectral resolution of ~4 cm^{-1}. Standard deviation on band positions is estimated at ±0.4 cm^{-1}.

Phases	***T (K)***	***P (MPa)***	***Component / assignment***					
			N_2 stretching		CO_2 (ν^-)[a]		CO_2 (ν^+)[a]	
			Position (cm^{-1})	FWHM (cm^{-1})	Position (cm^{-1})	Width (cm^{-1})	Position (cm^{-1})	Width (cm^{-1})
Gas[b]	284.6	3.6	2328.6	4.6	1285	4.6	1387.8	4.5
Type A	287.9	3.7	2323.6	4.3	1274.5	13	1381.4	10
Type B	287.3	3.7	2323.7	4.5	1276.4	11.6	1380.7	8

From these measurements, guest distributions within TBAB-*sc* structures can be revealed. The Raman signature of the encapsulated N_2 tends to be the most intense (relative to the contribution of the free gas) at a temperature close to that of dissociation (Figure 4). Although less conspicuous, the same behavior is observed for CO_2 (Figure 3). It becomes evident that the guest contribution of the guest in a type A structure

evolves with the temperature. Specifically, the Raman signatures corresponding to the guest cannot be clearly observed after 6h at 287.4 K (protocol 1, Figure 3 and 4) but appears gradually with time (protocol 2 in Figure 2 (t+72h), and in Figure 3 and 4). As noted above, type A is observed below the sample surface and mass transfer limitation of the gas phase to the hydrate phase may occur due to the presence of large crystals at 287.4 K that may hinder gas diffusion to the growing liquid/hydrate front (see optical image Figure 2, protocol 1). Therefore, a weak signal of the encapsulated N_2 is observed (Figure 4, protocol 1). In contrast, when the liquid phase is present mass transfers are facilitated (close to the dissociation limit at 287.9 K in protocol 1 or at 287.7 K in protocol 2), which could explain why Raman signatures for enclathrated CO_2 and N_2 are generally observed as more intense in type A (or type B) in this temperature range. Note that the contribution of the enclathrated guests in TBAB-*sc* structures, such as type B and its related polymorphs, is weak at high sub-cooling (281.1 K and 284.5 K) in protocol 2, whereas it is higher in protocol 1 (281.8 K and 284.5 K). We attribute this effect to the different protocols used for the formation of these TBAB-*sc*. In protocol 1 (cycling), the sample is subsequently cooled down (258 K) and heated up to 288.5 K many times, resulting in the partial dissociation and reformation of the *sc* hydrates. This process may favor mass transfers once TBAB-*sc* crystals are formed. In protocol 2, the sample is liquid during cooling (287 K) and TBAB-*sc* crystals form when approaching the low temperature of 266 K. Thus, the diffusion of the gas toward the growing hydrate/liquid front is hindered due to the formation of a solid hydrate layer that limits mass transfers from the moment hydrates have formed. Accordingly, mass transfers may increase only upon heating back to 287 K, i.e. close to dissociation temperature. It can thus be anticipated that this second protocol will not be as efficient as protocol 1 in capturing CO_2.

Compositional data derived from our Raman measurements can be found in supplementary material (Figure S2 and S3). It is shown that the final composition in the vapor phase is lower than the initial CO_2 composition (loading) of the CO_2-N_2 gas mixture, while the CO_2 composition in the hydrate reaches ~ 40%. This indicates that CO_2 is selectively entrapped during the *sc* formation process. Our results show that the hydrate composition is lower than the one found when starting from a 20% CO_2 + 80% N_2 gas mixtures with 40wt.% TBAB concentration [45]. Kim & Seo (2015) [45] reported that their flue gas analog is enriched to approximately a value of 60% in the *sc* hydrates. Thus, it seems likely that the resulting composition of CO_2 in the hydrate is dependent on the initial CO_2 content and also on the initial (high) salt concentration. Note that in comparison to canonical clathrates, *sc* hydrates performed better for the selective entrapment of CO_2 when the hydration process is applied to a gas mixture of the same initial composition (10% CO_2 + 90% N_2). Specifically, a CO_2 composition ranging from 25% to 40% was found in clathrates exhibiting structure type I [47], whereas a composition of 35 to 47 % was found in the present study, i.e. under much milder pressure and temperature conditions.

3.3. Selectivity in CO_2+N_2-TBAB-H_2O semi-clathrate hydrates

Quantitative estimates for hydrate selectivity are directly derived from the integrated areas of the distinct Raman signatures of each gas (CO_2 and N_2), either as a guest or as a free molecule. First is calculated the relative amount of CO_2 and N_2 in the gas phase ($y^G_{CO_2}/y^G_{N_2}$), with y_i^G the mole number of the component *i* in the free gas phase. Second is calculated the relative amount of guests in the hydrate phases with

$(z_{CO_2}^H / z_{N_2}^H)$, where z_i^H is the mole number of the component i in the hydrate phase. From these measurements, selectivity in the hydrates (separation factor S.F.) can be obtained from the following ratio [3,24]:

$$S.F. = \frac{\left(\frac{z_{CO_2}}{z_{N_2}}\right)_{Hyd}}{\left(\frac{y_{CO_2}}{y_{N_2}}\right)_{Gas}} \quad (1)$$

More information about this method has been detailed in our previous work [47].

Further analyses from these measurements are carried out by the study of the CO_2 concentration. The amount of CO_2 (concentration) in the gas phase can be calculated as follows:

$$Y_{CO_2} = \frac{y_{CO_2}^G}{y_{CO_2}^G + y_{N_2}^G} \quad (2)$$

Finally, the CO_2 concentration in the hydrate phase is derived as follows:

$$Z_{CO_2} = \frac{z_{CO_2}^H}{z_{CO_2}^H + z_{N_2}^H} \quad (3)$$

Figure 5 shows the comparison of the selectivity for the two protocols as a function of the different temperatures investigated and the different structures found at each step. Note that the selectivity in type A protocol 1 at 287.4 K cannot be determined due to the quasi-absence of guests in this structure (see discussion in the previous section). Figure 5 shows that two main parameters influence the resulting selectivity: first the type of structure, and second the protocol by which were formed the hydrates.

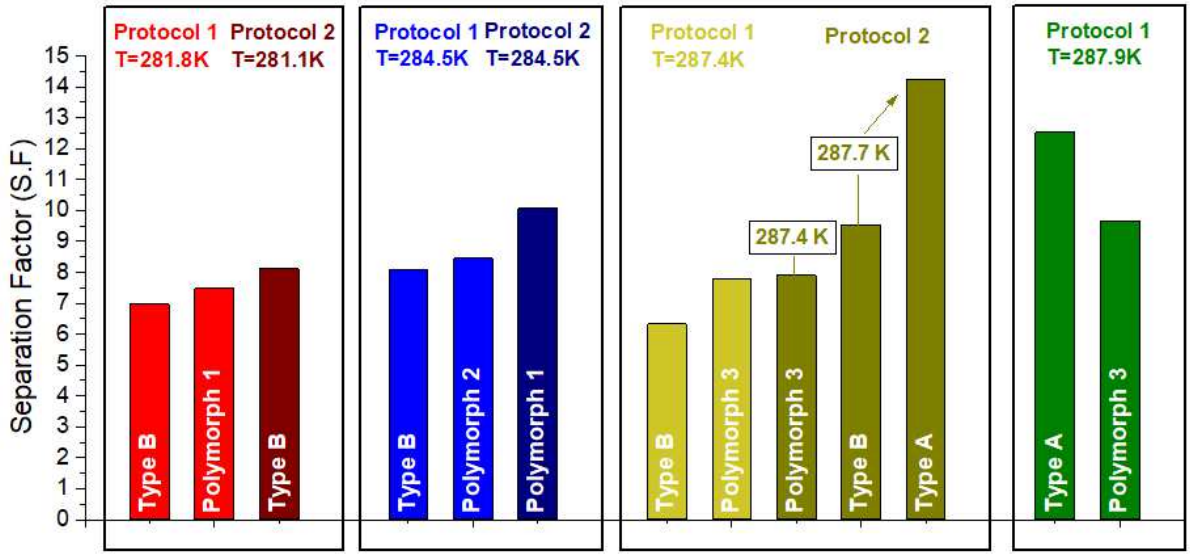

Figure 5: Comparison of the separation factors for both protocols at different temperatures. The selectivity is found to change according to the structure encountered at each temperature step in the different protocols (see text for details). Standard deviations for S.F. are estimated as ±1.7 in polymorphs and type B of protocol 1, ± 0.4 for type B of protocol 2, ± 0.5 in polymorphs of protocol 2.

Figure 5 shows that type B structures or related polymorphs (Poly 1 and Poly 2, Figure 2) feature a smaller selectivity (S.F. ~ 6.5 - 9.5) in comparison to type A structures or related polymorph Poly 3 (S.F. ~ 7.5 – 14.5). This finding suggests that structures such as type A may present themselves as a better solution for CCS development. A number of studies reported the selectivity of TBAB hydrates formed from an aqueous mixture containing low TBAB concentrations (often associated with the orthorhombic phase) [24,44,50–54]. This may be explained by the fact that the orthorhombic type B offers a better gas storage capacity in comparison to the tetragonal type A (~8.8wt.% in type A versus 11.5wt.% in type B, in mass% of CO_2) and a lower viscosity, which is important in gas system processing. However, since the incorporation of CO_2 (and N_2) drives the formation of distinct structures in comparison to the expected one without guests

[20,35], assessing the best initial TBAB concentration for optimal conditions for CCS development should not solely be based on information derived from simple guest-free TBAB-*sc*. Kim and Seo [45] measured the equilibrium composition in TBAB-*sc* starting from a 40 wt%TBAB aqueous solution (3.7 mol% TBAB) and a gas mixture of 20% CO_2 + 80% N_2. Although not reported, it is possible to estimate the selectivity in their sample using the compositional data provided. A S.F. of ~7-8 can be derived at T = 275 K (ΔT_{sub} =5 K) and p = 3.0 MPa. Their results are in remarkable good agreement with S.F. derived from our Raman data (S.F. between 7 and 9 depending on the structure) at an equivalent sub-cooling (ΔT_{sub} ~ 6 K in our case). However, the authors reported that type A (tetragonal phase) has formed in their process and that encapsulation of the guest did not modify the empty–TBAB-*sc* structure [45]. Their assumption may not be entirely correct based on the signature of their Raman spectra that show a double peak at 1310 cm^{-1} and 1328 cm^{-1} in their TBAB-*sc* structures, characteristic of type B (Figure 3) [20]. In contrast, type A features a broad asymmetric band shape in this region (Figure 3). Therefore, we hypothesize that they have formed instead a structure type B (or one of its related polymorphs Poly 1 or Poly 2), hence affecting the resulting S.F. which would end up being not as high as the one expected for a tetragonal phase (type A) only accessible at much lower sub-cooling (Figure 2 and 5).

Furthermore, the separation factor is always found higher in protocol 2 than in protocol 1. Thus, a slower formation process such as the one adopted in the isochoric pressure search method (protocol 2) seems more efficient at selecting CO_2. However, even the highest values obtained here are lower than the values reported by Hashimoto et al., (2017) [24]. They obtained S.F. between 1.4 and 21.9 using a closed static reactor where the formation was done at two TBAB concentrations (32 wt.% and 20 wt.%). They also

performed a continuous gas flow separation but did not determine the resulting selectivity. The time of equilibration of their system was ~20-28 h and the initiation of hydrates formation was obtained with a soft stirring of the solution (to improve gas dissolution) at p ~ 1, 2 and 3 MPa and a sub-cooling of 2-3.5 K at T = 282.2 K or 285.2 K. In a companion paper [44], the authors reported S.F. values much lower for the same system under the same p, T conditions: between 4 and 5.7, which are closer to the results obtained here for protocol 1. Hydrate promotion was performed in this latter case by cooling the system down to 260 K and inserting a metal rod quenched by liquid nitrogen [44]. The equilibration time in this study was 20 h. This latter protocol may correspond to the fast cooling approach of our protocol 1 due to the quenching procedure. When comparing the two methods and the resulting SF values, it seems that the initial formation conditions impact the selectivity, as observed in our work with protocols 1 and 2 however less pronounced. From our observations, it seems that a fast cooling procedure hinders the incorporation of CO_2 guests relative to N_2. However, sufficient equilibration time should mitigate this effect. Other groups reported values of 5.3-7.3 for selectivity factors (S.F) in the low TBAB concentration regime (w= 0.05, p = 4.3 MPa, 20%CO_2+80%N_2, Li et al., 2009, [53]), while a SF of 13 was reported when increasing the TBAB concentration at 10wt.% and 15wt.% in a CO_2-N_2 mixture of 17%CO_2+83%N_2 [54]. This shows that not only the crystallization parameters (p, ΔT_{sub}) influence the selectivity, but also the initial concentration of both the flue gas phase and the salt.

In both protocols, structure type A emerges when approaching the dissociation temperature, and this structure shows better selectivity in comparison to the other TBAB-*sc* structures even though the theoretical amount of gas captured is known to be less than in type B [20]. More generally, the amount of gas captured

is less in TBAB-*sc* structures than in canonical clathrate structures, but the higher selectivity in semi-clathrates may confer greater performance for CO_2 removal from the gas phase in comparison to canonical clathrates [24]. At deep sub-cooling of ~13 K, most TBAB-*sc* crystals are empty (with no or only a small amount of guest-gases trapped in the cavities), as the dissolution of the guests is mainly limited by the high concentration of dissolved TBAB. Upon annealing, the sample surface starts to form TBAB-*sc* crystals filled with CO_2 and N_2 guests and TBAB is removed from the solution to participate in hydrates formation (type B, with a high hydration number). The remaining solution below the surface has mainly crystallized into a type A (with no or very little guest), as it is not directly exposed to the gaseous species. At lower sub-cooling (~1 K), i.e., when approaching dissociation, the empty–TBAB-*sc* phase (type A with no guest) becomes metastable above 286 K. Type A guest-free TBAB-*sc* probably release TBAB in the solution for the preferential formation of type A, which crystallizes with the preferential capture of CO_2. A rough estimate of the amount of CO_2 captured during the formation process can be evaluated from our data. For this purpose, we used the procedure reported in Chazallon & Pirim, 2018 [47], where we combined our Raman and PVT data to derive the recovery fraction (fraction of CO_2 in the hydrate phase relative to that in the feed gas phase), and that we calculated to be ~34%. This value is lower than the one found in canonical hydrates (without TBAB), which is ≥ ~37% depending on the starting conditions[3,47]. In comparison, Li et al., 2012 [54] derived a maximal CO_2 recovery fraction (split fraction, S.Fr.) of ~46% in their TBAB samples. Although details about the structure were unknown, they assumed they had formed the orthorhombic type B structure starting from a TBAB concentration of 10% and a gas mixture of (17% CO_2 + 83% N_2). While their S.Fr. is higher, their maximal S.F. is smaller (~13) than ours (~14). This illustrates the importance of finding

the most suitable operating conditions to optimize HBSP, and highlights how necessary it is to determine the two performance parameters, i.e. S.Fr. and S.F, to have a full description of the CO_2 gas consumption and CO_2 separation.

5. CONCLUSIONS

Our analyses provided new insights into the performance of the CO_2 capture process for developing HBSP using ionic clathrate hydrates. The contact between a gas mixture containing 10% CO_2 + 90 % N_2 and an aqueous solution of TBAB (35wt.% TBAB) forms semi-clathrates and selectively removes CO_2 from the gas phase. The performance of distinct formation protocols widely used in the literature for hydrate formation is evaluated from a selectivity standpoint. The structure, selectivity and equilibrium properties are studied *in-situ* with optical microscopy and Raman spectroscopy in a high-pressure reactor at 3.7 MPa and temperatures approaching dissociation. In addition, the temperature dependencies of the surface morphology and the molecular structures are obtained from a detailed comparison of optical images and Raman spectra.

First, a new dissociation point is determined at 287.8 ± 0.3 K, in both protocols. In line with our previous findings [20], the encapsulation of guest gases stabilizes structure type B (and its related polymorph: Poly 1 in protocol 1) at high sub-cooling, although type A (tetragonal) is the expected stable phase in guest-free TBAB semi-clathrates with a TBAB concentration of 35 wt.%. *In-situ* Raman spectra of TBAB-*sc* show that type B remains stable up to 287.7 K as dissociation approaches, while a succession of polymorphic transformations can be followed concomitantly between ~281 K and ~287.8 K in both protocols. CO_2 selectivity tends to reduce slightly when approaching dissociation, except when very close to

the dissociation temperature where type A is formed. Structure type A shows a much higher selectivity than either type B or all other successive polymorphs. It has been assumed earlier that CO_2 selectivity degrades as the driving force for hydrate formation decreases [44]. Our results show that this holds true as long as type A is not formed. Furthermore, Type B is promoted at the gas-hydrate interface at high sub-cooling, whereas type A (without guests (at high sub-cooling) and with guests (at small sub-cooling)) is observed in the bulk below the surface. Finally, hydrate surface morphology undergoes continuous changes during sample annealing, starting from a rough surface coated with polygonal or stacked shaped crystals to the formation of columnar TBAB-*sc* crystals close to the dissociation when sufficient time is allowed. The detailed relationship between molecular structure (with the formation of complex polymorphs) and crystal morphology needs however to be further investigated.

One interesting outcome of our analysis observed in both protocols is that while variable performances on CO_2 selectivity are obtained at high sub-cooling (protocol 2 performs slightly better than protocol 1 in terms of selectivity), better performance is obtained when approaching the dissociation temperature, with selectivity factors reaching greater and almost identical values in both protocols, depending however upon the structure of TBAB semi-clathrates crystals. This work highlights also the remarkably slow formation rates for such hydrates, as pointed out in a couple of other studies [37,55].

AUTHOR CONTRIBUTIONS

C. T. Rodriguez and B. Chazallon conceived and designed the experiments; C. T. Rodriguez, Q. D. Le, and B. Chazallon performed the experiments; C. T. Rodriguez, C. Focsa, C. Pirim and B. Chazallon analyzed the

data; C. T. Rodriguez wrote the original draft preparation; C. Pirim, C. Focsa and B. Chazallon wrote, reviewed and edited the draft.

FUNDING

This research was supported by the Université de Lille and the Région Hauts-de-France with a PhD grant n°17006757.

ACKNOWLEDGMENTS

The authors acknowledge the Région Hauts-de-France, the Ministère de l'Enseignement Supérieur et de la Recherche and the European Fund for Regional Economic Development for their financial support (CPER CLIMIBIO). The authors also acknowledge funding from the Interreg 2 Seas programme 2014-2020 co-funded by the European Regional Development Fund under subsidy contract Carbon2Value 2S01-094.

CONFLICTS OF INTEREST

The authors declare no conflict of interest.

REFERENCES

[1] M. Bui, C.S. Adjiman, A. Bardow, E.J. Anthony, A. Boston, S. Brown, P.S. Fennell, S. Fuss, A. Galindo, L.A. Hackett, J.P. Hallett, H.J. Herzog, G. Jackson, J. Kemper, S. Krevor, G.C. Maitland, M. Matuszewski, I.S. Metcalfe, C. Petit, G. Puxty, J. Reimer, D.M. Reiner, E.S. Rubin, S.A. Scott, N. Shah, B. Smit, J.P.M. Trusler, P. Webley, J. Wilcox, N. Mac Dowell, Carbon capture and storage (CCS): The way forward, Energy Environ. Sci. 11 (2018) 1062–1176. doi:10.1039/c7ee02342a.

[2] R.B. Jackson, C. Le Quéré, R.M. Andrew, J.G. Canadell, J.I. Korsbakken, Z. Liu, G.P. Peters, B.

Zheng, Global energy growth is outpacing decarbonization, Envirom. Res. Lett. 13 (2018) 120401. doi:10.1088/1748-9326/aaf303.

[3] P. Linga, R. Kumar, P. Englezos, The clathrate hydrate process for post and pre-combustion capture of carbon dioxide, J. Hazard. Mater. 149 (2007) 625–629. doi:10.1016/j.jhazmat.2007.06.086.

[4] B. Li, Y. Duan, D. Luebke, B. Morreale, Advances in CO2 capture technology: A patent review, Appl. Energy. 102 (2013) 1439–1447. doi:10.1016/j.apenergy.2012.09.009.

[5] P. Luis, Use of monoethanolamine (MEA) for CO2 capture in a global scenario: Consequences and alternatives, Desalination. 380 (2016) 93–99. doi:10.1016/j.desal.2015.08.004.

[6] S. Oh, M. Binns, H. Cho, J. Kim, Energy minimization of MEA-based CO2 capture process, Appl. Energy. 169 (2016) 353–362. doi:10.1016/j.apenergy.2016.02.046.

[7] N. Xie, B. Chen, C. Tan, Z. Liu, Energy Consumption and Exergy Analysis of MEA-Based and Hydrate-Based CO2 Separation, Ind. Eng. Chem. Res. 56 (2017) 15091–15101. doi:10.1021/acs.iecr.7b03729.

[8] C. Yu, C. Huang, C. Tan, A Review of CO2 Capture by Absorption and Adsorption, Aerosol Air Qual. Res. (2012) 745–769. doi:10.4209/aaqr.2012.05.0132.

[9] Y. Wang, L. Zhao, A. Otto, M. Robinius, D. Stolten, A Review of Post-combustion CO2 Capture Technologies from Coal-fired Power Plants, Energy Procedia. 114 (2017) 650–665. doi:10.1016/j.egypro.2017.03.1209.

[10] E. Favre, Carbon dioxide recovery from post-combustion processes: Can gas permeation membranes compete with absorption?, J. Memb. Sci. 294 (2007) 50–59. doi:10.1016/j.memsci.2007.02.007.

[11] A.A. Olajire, CO2 capture and separation technologies for end-of-pipe applications - A review, Energy. 35 (2010) 2610–2628. doi:10.1016/j.energy.2010.02.030.

[12] H. Yang, Z. Xu, M. Fan, R. Gupta, R.B. Slimane, A.E. Bland, I. Wright, Progress in carbon dioxide separation and capture: A review, J. Environ. Sci. 20 (2008) 14–27.

[13] D. Berstad, R. Anantharaman, P. Nekså, Low-temperature CO2 capture technologies - Applications and potential, Int. J. Refrig. 36 (2013) 1403–1416. doi:10.1016/j.ijrefrig.2013.03.017.

[14] D.M. D'Alessandro, B. Smit, J.R. Long, Carbon Dioxide Capture: Prospects for New Materials Angewandte, Angew. Chem. Int. (2010) 6058–6082. doi:10.1002/anie.201000431.

[15] D.E. Sloan, C.A. Koh, Clathrate Hydrates of Natural Gases, 3rd ed., CRC Press, Boca Raton, FL, 2008.

[16] G.A. Jeffrey, Hydrate inclusion compounds, J. Incl. Phenom. 1 (1984) 211–222. doi:10.1007/BF00656757.

[17] W. Shimada, M. Shiro, H. Kondo, S. Takeya, H. Oyama, E. Takao, H. Narita, Tetra-n-butylammonium bromide-water, Acta Cryst. C61 (2005) o65–o66. doi:10.1107/S0108270104032743.

[18] D.L. Fowler, W. V Loebenstein, D.B. Pall, C.A. Kraus, Some Unusual Hydrates of Quaternary Ammonium Salts, J. Am. Chem. Soc. 62 (1940) 1140–1142.

[19] W. Shimada, T. Ebinuma, H. Oyama, Y. Kamata, S. Takeya, T. Uchida, J. Nagao, H. Narita, Separation of Gas Molecule Using Tetra-n-butyl Ammonium Bromide Semi-Clathrate Hydrate Crystals Separation of Gas Molecule Using Tetra-n-butyl Ammonium Bromide Semi-Clathrate Hydrate Crystals, Jpn. J. Appl. Phys. 42 (2003) L129–L131. doi:10.1143/JJAP.42.L129.

[20] B. Chazallon, M. Ziskind, Y. Carpentier, C. Focsa, CO2 Capture Using Semi-Clathrates of Quaternary Ammonium Salt : Structure Change Induced by CO2 and N2 Enclathration, J. Phys. Chem. 118 (2014) 13440–13452. doi:dx.doi.org/10.1021/jp507789z.

[21] V. Belandria, A.H. Mohammadi, A. Eslamimanesh, D. Richon, M.F. Sánchez-mora, L.A. Galicia-luna, Phase equilibrium measurements for semi-clathrate hydrates of the (CO2 + N2 + tetra-n-butylammonium bromide) aqueous solution systems: Part 2, Fluid Phase Equilib. 322–323 (2012) 105–112. doi:10.1016/j.fluid.2012.02.020.

[22] S. Lee, S. Park, Y. Lee, J. Lee, H. Lee, Y. Seo, Guest Gas Enclathration in Semiclathrates of Tetra-n-butylammonium Bromide: Stability Condition and Spectroscopic Analysis, Langmuir. 27 (2011) 10597–10603. doi:dx.doi.org/10.1021/la202143t.

[23] M.V. Chary, N.C. Keerthysri, S.V.N. Vupallapati, N. Lingaiah, S. Kantevari, Tetrabutylammonium bromide (TBAB) in isopropanol : An efficient , novel , neutral and recyclable catalytic system for the synthesis of 2 , 4 , 5-trisubstituted imidazoles, 9 (2008) 2013–2017. doi:10.1016/j.catcom.2008.03.037.

[24] H. Hashimoto, T. Yamaguchi, T. Kinoshita, Gas separation of flue gas by tetra-n-butylammonium bromide hydrates under moderate pressure conditions, Energy. 129 (2017) 292–298. doi:10.1016/j.energy.2017.04.074.

[25] A.H. Mohammadi, A. Eslamimanesh, V. Belandria, D. Richon, Phase Equilibria of Semiclathrate Hydrates of CO2, N2, CH4, or H2 + Tetra-n-butylammonium Bromide Aqueous Solution, J. Chem. Eng. Data. 56 (2011) 3855–3865. doi:dx.doi.org/10.1021/je2005159.

[26] S. Takeya, S. Muromachi, T. Maekawa, Y. Yamamoto, H. Mimachi, T. Kinoshita, T. Murayama, H. Umeda, D.-H. Ahn, Y. Iwasaki, H. Hashimoto, T. Yamaguchi, K. Okaya, S. Matsuo, Design of Ecological CO2 Enrichment System for Greenhouse Production using TBAB + CO2 Semi-Clathrate Hydrate, Energies. 10 (2017) 927. doi:10.3390/en10070927.

[27] H. Dashti, L.Z. Yew, X. Lou, Advances in gas hydrate-based CO2 capture, J. Nat. Gas Sci. Eng. 23 (2015) 195–207. doi:10.1016/j.jngse.2015.01.033.

[28] R. Mcmullan, G.A. Jeffrey, Hydrates of the Tetra nbutyl and Tetra iamyl Quaternary Ammonium Salts Hydrates of the Tetra n-butyl and Tetra i-amyl Quaternary Ammonium Salts, J. Chem. Phys. 31 (1959) 1231–1234. doi:10.1063/1.1730574.

[29] J. Lipkowski, V.Y. Komarov, T. V Rodionova, Y.A. Dyadin, L.S. Aladko, The Structure of Tetrabutylammonium Bromide Hydrate (C4H9)4NBr·21/3H2O, J. Supramol. Chem. 2 (2002) 435–439. doi:10.1016/S1472-7862(03)00054-6.

[30] H. Oyama, W. Shimada, T. Ebinuma, Y. Kamata, S. Takeya, T. Uchida, J. Nagao, H. Narita, Phase diagram, latent heat, and specific heat of TBAB semiclathrate hydrate crystals, Fluid Phase Equilib. 234 (2005) 131–135. doi:10.1016/j.fluid.2005.06.005.

[31] T. V Rodionova, V.Y. Komarov, G. V Villevald, T.D. Karpova, N. V Kuratieva, A.Y. Manakov, T. V Rodionova, V.Y. Komarov, G. V Villevald, T.D. Karpova, Calorimetric and Structural Studies of Tetrabutylammonium Bromide Ionic Clathrate Hydrates Calorimetric and Structural Studies of Tetrabutylammonium Bromide Ionic Clathrate Hydrates, J. Phys. Chem B. 117 (2013) 10677–10685. doi:10.1021/jp406082z.

[32] K. Sato, H. Tokutomi, R. Ohmura, Phase equilibrium of ionic semiclathrate hydrates formed with tetrabutylammonium bromide and tetrabutylammonium chloride, Fluid Phase Equilib. 337 (2013) 115–118. doi:10.1016/j.fluid.2012.09.016.

[33] M. Oshima, M. Kida, J. Nagao, Hydration numbers and thermal properties of tetra-n-butyl ammonium bromide semiclathrate hydrates determined by ion chromatography and differential scanning calorimetry, J. Chem. Thermodyn. 123 (2018) 32–37. doi:10.1016/j.jct.2018.03.018.

[34] W. Shimada, T. Ebinuma, H. Oyama, Y. Kamata, H. Narita, Free-growth forms and growth kinetics of tetra-n-butyl ammonium bromide semi-clathrate hydrate crystals, J. Cryst. Growth. 274 (2005) 246–250. doi:10.1016/j.jcrysgro.2004.09.071.

[35] S. Muromachi, K.A. Udachin, K. Shin, S. Alavi, I.L. Moudrakovski, R. Ohmura, J.A. Ripmeester, Guest-induced symmetry lowering of an ionic clathrate material for carbon capture, Chem. Commun. 50 (2014) 11476–11479. doi:10.1039/c4cc02111h.

[36] Y. Jin, J. Nagao, Change in the stable crystal phase of tetra-n-butylammonium bromide (TBAB) hydrates enclosing xenon, J. Phys. Chem. C. 117 (2013) 6924–6928. doi:10.1021/jp310441u.

[37] X. Zhou, Z. Long, C. Tang, D. Liang, Kinetic Measurements on CO2 Hydrate Formation in the Presence of Tetra-n-butyl Ammonium Bromide, Energy & Fuels. 32 (2018) 9683–9691. doi:10.1021/acs.energyfuels.8b01914.

[38] P. Babu, P. Linga, R. Kumar, P. Englezos, A review of the hydrate based gas separation (HBGS) process forcarbon dioxide pre-combustion capture, Energy. 85 (2015) 261–279. doi:10.1016/j.energy.2015.03.103.

[39] M.K. Mondal, H.K. Balsora, P. Varshney, Progress and trends in CO2 capture/separation technologies: A review, Energy. 46 (2012) 431–441. doi:10.1016/j.energy.2012.08.006.

[40] M. Arjmandi, A. Chapoy, B. Tohidi, Equilibrium Data of Hydrogen, Methane, Nitrogen, Carbon Dioxide, and Natural Gas in Semi-Clathrate Hydrates of Tetrabutyl Ammonium Bromide, J. Chem.

Eng. Data. 52 (2007) 2153–2158. doi:10.1021/je700144p.

[41] J. Deschamps, D. Dalmazzone, Dissociation enthalpies and phase equilibrium for TBAB semi-clathrate hydrates of N2, CO2, N2 + CO2 and CH4 + CO2, J. Therm. Anal. Calorim. 98 (2009) 113–118. doi:10.1007/s10973-009-0399-3.

[42] A. Eslamimanesh, A.H. Mohammadi, D. Richon, P. Naidoo, D. Ramjugernath, Application of gas hydrate formation in separation processes: A review of experimental studies, J. Chem. Thermodyn. 46 (2012) 62–71. doi:10.1016/j.jct.2011.10.006.

[43] P. Meysel, L. Oellrich, P.R. Bishnoi, M.A. Clarke, Experimental investigation of incipient equilibrium conditions for the formation of semi-clathrate hydrates from quaternary mixtures of (CO2 + N2 + TBAB + H2O), J. Chem. Thermodyn. 43 (2011) 1475–1479. doi:10.1016/j.jct.2011.04.021.

[44] H. Hashimoto, T. Yamaguchi, H. Ozeki, S. Muromachi, Structure-driven CO2 selectivity and gas capacity of ionic clathrate hydrates, Sci. Rep. (2017) 1–10. doi:10.1038/s41598-017-17375-1.

[45] S. Kim, Y. Seo, Semiclathrate-based CO2 capture from flue gas mixtures: An experimental approach with thermodynamic and Raman spectroscopic analyses, Appl. Energy. 154 (2015) 987–994. doi:10.1016/j.apenergy.2015.05.107.

[46] B. Chazallon, CO2 Capture by Gas Hydrate Crystallization : Investigation of Equilibrium and Compositional Properties of CO2-N2 Hydrates by Micro-Raman Spectroscopy, Phys. Chem. Ice 2010. (2011) 173–181.

[47] B. Chazallon, C. Pirim, Selectivity and CO2 capture efficiency in CO2-N2 clathrate hydrates investigated by in-situ Raman spectroscopy, Chem. Eng. J. 342 (2018) 171–183. doi:10.1016/j.cej.2018.01.116.

[48] Z. Long, X. Zhou, X. Shen, D. Li, D. Liang, Phase Equilibria and Dissociation Enthalpies of Methane Hydrate in Imidazolium Ionic Liquid Aqueous Solutions, Ind. Eng. Chem. Res. 54 (2015) 11701–11708. doi:10.1021/acs.iecr.5b03480.

[49] S. Lee, Y. Lee, S. Park, Y. Seo, Phase Equilibria of Semiclathrate Hydrate for Nitrogen in the Presence of Tetra-n-butylammonium Bromide and Fluoride, J. Chem. Eng. Data. 55 (2010) 5883–5886.

[50] N. Ye, P. Zhang, Equilibrium data and morphology of tetra-n-butyl ammonium bromide semiclathrate hydrate with carbon dioxide, J. Chem. Eng. Data. 57 (2012) 1557–1562. doi:10.1021/je3001443.

[51] S. Kim, I.H. Baek, J.K. You, Y. Seo, Guest gas enclathration in tetra-n-butyl ammonium chloride (TBAC) semiclathrates: Potential application to natural gas storage and CO2 capture, Appl. Energy. 140 (2015) 107–112. doi:10.1016/j.apenergy.2014.11.076.

[52] S. Fan, S. Li, J. Wang, X. Lang, Y. Wang, Efficient capture of CO2 from simulated flue gas by formation of TBAB or TBAF semiclathrate hydrates, Energy and Fuels. 23 (2009) 4202–4208.

doi:10.1021/ef9003329.

[53] S. Li, S. Fan, J. Wang, X. Lang, CO2 capture from binary mixture via forming hydrate with the help of tetra-n -butyl ammonium bromide, J. Nat. Gas Chem. 18 (2009) 15–20. doi:10.1016/S1003-9953(08)60085-7.

[54] X. Li, H. Zhan, C. Xu, Z. Zeng, Q. Lv, Effects of Tetrabutyl- (ammonium / phosphonium) Salts on Clathrate Hydrate Capture of CO2 from Simulated Flue Gas, Energy Fuels. 26 (2012) 2518–2527. doi:© 2012 American Chemical Society 2518 dx.doi.org/10.1021/ef3000399.

[55] H. Hayama, H. Akiba, Y. Asami, R. Ohmura, Crystal growth of ionic semiclathrate hydrate formed at interface between CO2+N2 gas mixture and tetrabutylammonium bromide aqueous solution, Koren J. Chem. Eng. 33 (2016) 1942–1947. doi:10.1007/s11814-016-0035-4.